


A Metamaterial-Coupled Wireless Power Transfer System Based on Cubic High-Dielectric Resonators

Rupam Das , Abdul Basir , *Student Member, IEEE*, and Hyongsuk Yoo , *Member, IEEE*

Abstract—In this paper, a metamaterial-coupled, highly efficient, miniaturized, and long-range wireless power transfer (WPT) system based on a cubic high-dielectric resonator (CHDR) is explored. The proposed WPT system consists of two CHDR metamaterials separated by a distance and excited by two rectangular coils. Initially, this WPT system is analyzed by considering the cube dielectric permittivity, $\epsilon_r = 1000$, and loss tangent, $\tan\delta = 0.00001$. From the Ansoft HFSS simulation, it is observed that the system operates in the hybrid resonance mode resonating as a horizontal magnetic dipole providing more than 90% power transfer efficiency at a distance of 0.1λ . In addition, parametric studies regarding the transmitter and receiver sizes, loss tangent, receiver misorientation, cube periodicity, etc., are carried out. One of the significant findings of this parametric study reveals that the suggested WPT system is less sensitive to the displacement of the receiver coil, and the WPT efficiency due to misorientation of the receiver can be increased by changing the CHDR cube rotation. Due to inaccessibility of the very high $\epsilon_r = 1000$, 18 microwave ceramic samples of EXXELIA TEMEX E5080 (Oxide composition: Ba Sm Ti), which has a permittivity, $\epsilon_r = 78$, permeability, $\mu_r = 1$, and a loss tangent, $\tan\delta = 0.0004$, was made for experimental verification. These cubes are surrounded by Teflon to make the CHDR resonators. From simulations and measurements, it is found that the proposed system outperforms the most recent high-dielectric or copper-based WPT systems in terms of efficiency, range, size, and specific absorption rate.

Index Terms—Cubic high-dielectric resonator (CHDR), hybrid resonance mode, magnetic dipole (MD), metamaterial (MTM), rectifier, specific absorption rate (SAR), wireless power transfer (WPT).

I. INTRODUCTION

WIRELESS power transfer (WPT) makes it possible to supply power through an air gap, without the need for

Manuscript received June 19, 2018; revised September 21, 2018; accepted October 18, 2018. Date of publication November 7, 2018; date of current version April 30, 2019. This work was supported by the National Research Foundation of Korea through the Basic Science Research Program funded by the Ministry of Education, Science and Technology under Grant NRF – 2019R1A2C2004774. (Corresponding author: Hyongsuk Yoo.)

R. Das is with the Department of Engineering, University of Glasgow, G12 8QQ Glasgow, Scotland, U.K. (e-mail: rupam.das@glasgow.ac.uk).

A. Basir and H. Yoo are with the Department of Biomedical Engineering, Hanyang University, Seoul 04763, Republic of Korea (e-mail: engrbasir@gmail.com; hsyoo@hanyang.ac.kr).

Color versions of one or more of the figures in this paper are available online at <http://ieeexplore.ieee.org>.

Digital Object Identifier 10.1109/TIE.2018.2879310

current-carrying wires [1]. WPT can provide power from an alternating current source to compatible batteries or devices without physical connectors or wires. WPT can recharge mobile phones and tablets [2], drones, cars, implantable devices [3], and even transportation equipment [4], [5]. The concept of transferring power without wires, however, has been around since the late 1890s [6]. Since then, many research groups have been working on this problem, and different methodologies have been introduced to WPT systems. One of the issues being addressed is analyzing and optimizing the near-field inductive or magnetic resonance coupling WPT [7]–[10]. Another is improving the power control capability and the WPT efficiency [11]–[18]. Miniaturization of the transmitter and receiver coil is also a major concern [3], [19], [20]. Furthermore, a longer transfer distance and more flexible adaption are required for numerous mobile devices [9], [17], [20], [21].

One of the nonradiative power transfer techniques is based on resonant coupling between the same-frequency resonators, where the power is transferred through the overlap of their near fields. In 2007, a group from the Massachusetts Institute of Technology experimentally transferred the power of 60 W over a distance of 2 m with 45% efficiency *via* strongly coupled magnetic resonances between two metallic coils [7]. However, the resonance-coupling-based WPT system is very sensitive to the receiver and transmitter sizes, orientations, and positions [22], [23]. The possibility of omnidirectional WPT has also been explored, as opposed to the use of one direction or two directions on the same plane [24]. However, the proposed system in [24] yields only 60% efficiency at a distance of 0.013λ , which leaves much to be desired. Recently, WPT systems based on high-permittivity dielectric resonator coupling have been experimentally tested [25], [26]. As described in [25], this high-permittivity dielectric introduced a higher order magnetic quadruple (MQ) mode, which offers high WPT efficiency even with a random orientation between the transmitter and the receiver. The same group extended their work in another study [26] by incorporating a colossal permittivity dielectric ($\epsilon_r = 1000$ and $\tan\delta = 0.00025$) at 232 MHz. By applying an impedance matching technique, an efficiency of 50% was achieved within the separation between the resonators $d = 16$ cm (0.125λ).

To increase the power transfer efficiency, researchers have also demonstrated that a metamaterial (MTM) three-dimensional (3-D)/metasurface two-dimensional (2-D) lens or slab can be used [13], [14], [17], [18], [21], [27]–[29]. MTMs

are artificial materials composed of engineered structures that possess peculiar electromagnetic properties not seen in natural materials, such as negative refractive indexes and evanescent wave amplification [28], [30]. Bearing in mind that the magnetic-resonant-coupling-based WPT is essentially coupling of evanescent waves, MTM can be used to enhance the WPT efficiency. On one hand, the efficiency of the WPT system with the MTM is considerably improved for adaptive charging. On the other hand, it can increase the flexibility of the operating range for telemetry systems, such as a farther transfer distance and larger misalignment tolerance for electronic or implantable devices [14]. In most of the previous studies [14], [17], [18], [21], [28], [29], a copper-based MTM/metamaterial slab was placed between the transmitter and the receiver to improve the WPT system. However, the polarization dependence of the MTM poses a major drawback. Furthermore, copper-based MTMs introduce ohmic losses at very high frequency and lower the quality factor (Q-factor) of the system as well as the efficiency. In contrast, resonant dielectric structures operating as dielectric resonator antennas (DRAs) *via* displacement currents can be virtually free from ohmic loss, making them intrinsically highly efficient [25], [26]. Furthermore, subwavelength DRAs with moderate permittivities ($\epsilon_r > 5$) can efficiently support different modes of resonance [25]. One important and useful mode is pure magnetic resonance, which cannot be obtained with single-layer metallic resonators.

In this paper, an MTM-coupled, highly efficient, miniaturized, and long-range WPT system based on a cubic high-dielectric resonator (CHDR) is explored. The CHDR is an MTM with CHDRs in a cubic lattice embedded in a low-dielectric background. This MTM was proposed in [31], in which the authors made use of a combination of Mie resonance and Bragg scattering to achieve the MTM properties [32], [33]. Since the efficiency of WPT systems has been improved with high-permittivity dielectric coupling, it is expected that the WPT efficiency can be further improved by using all-dielectric MTM coupling. To the best of our knowledge, there are no previous studies regarding the high-dielectric MTM-coupled WPT system. The rest of this paper is structured as follows. Section II analyzes the suggested WPT system by considering the unit cell of the CHDR and CHDR MTM properties and by characterizing the MTM-coupled WPT system. A comparison among previous studies and this paper in terms of efficiency, WPT system size, and loss tangent variations is also included in this section. Parametric studies of the MTM-coupled WPT system are discussed. The influence on WPT efficiency owing to parameters such as the cube lattice periodicity, separation between the transmitter and CHDR, transmitter and receiver sizes, number of arrays, and receiver misalignment is addressed in Section III. Section IV comprises the experimental demonstration of the proposed WPT system. Two CHDR MTMs were made by using 18 high-dielectric cubes ($\epsilon_r = 78$ and $\tan\delta = 0.0004$) surrounded by Teflon. The specific absorption rate (SAR) is numerically calculated, and improvement in the WPT efficiency in the presence of a saline phantom for the proposed WPT system is experimentally demonstrated. Finally, the versatility of the proposed WPT system is presented by taking into account the receiver misalignment.

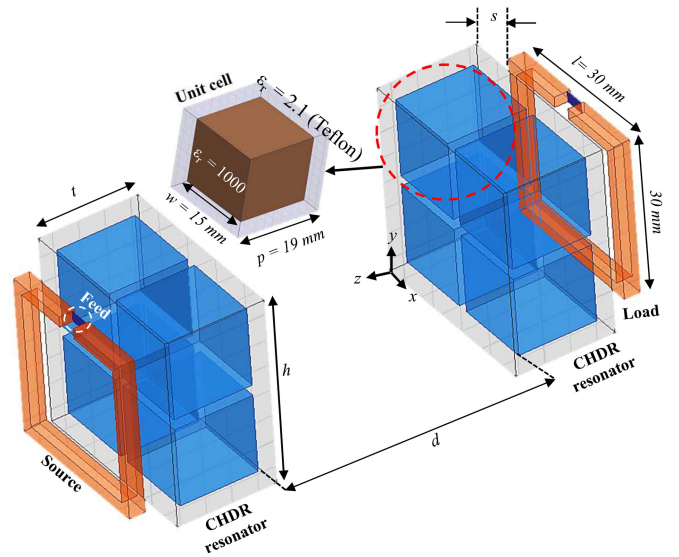


Fig. 1. (a) Schematic of the proposed CHDR MTM-based WPT system.

II. ANALYSIS OF THE PROPOSED WPT SYSTEM

A schematic of the proposed WPT system is shown in Fig. 1. The system consists of two rectangular CHDR MTM resonators separated at a distance, d . For clarification, the WPT system will be divided into the following three sections: unit cell consideration, CHDR MTM characterization, and WPT system characterization.

A. Unit Cell Consideration

1) Theoretical Background: The proposed WPT system along with the unit cell of the CHDR structure is shown in Fig. 1. Theoretically, a rectangular cavity resonator with a metal wall has the resonant frequencies given by

$$f_{mnp} = \frac{1}{2\sqrt{\epsilon\mu}} \sqrt{\left(\frac{m}{s}\right)^2 + \left(\frac{n}{t}\right)^2 + \left(\frac{p}{w}\right)^2}. \quad (1)$$

where integers m , n , and p denote the number of half-wave variations in the x -, y -, and z -directions, respectively, and s , t , and w represent the dimensions of the rectangular cavity, respectively. If a cubic cavity resonator is chosen, then all lengths are equal, which means $s = t = w$. In the case of such a cavity resonator, all the lowest order modes such as TM₁₁₀, TE₀₁₁, and TE₁₀₁ have the same field patterns or frequency and referred as the degenerate modes. The resonant frequency of these degenerate modes is

$$f = \frac{1}{\sqrt{2\epsilon\mu}w}. \quad (2)$$

In the case of a high-dielectric resonator, boundary conditions at the walls can be considered as an open circuits [31]; hence, resonant frequencies of the modes can also be approximated by (1) and (2). It is found that if a unit cell undergoes electric and magnetic resonances simultaneously, it might demonstrate a polarization-invariant response due to superimposition of the two resonant modes [34]. The CHDR has degenerate TE and TM modes due to cubic nature of the 3-D structure according

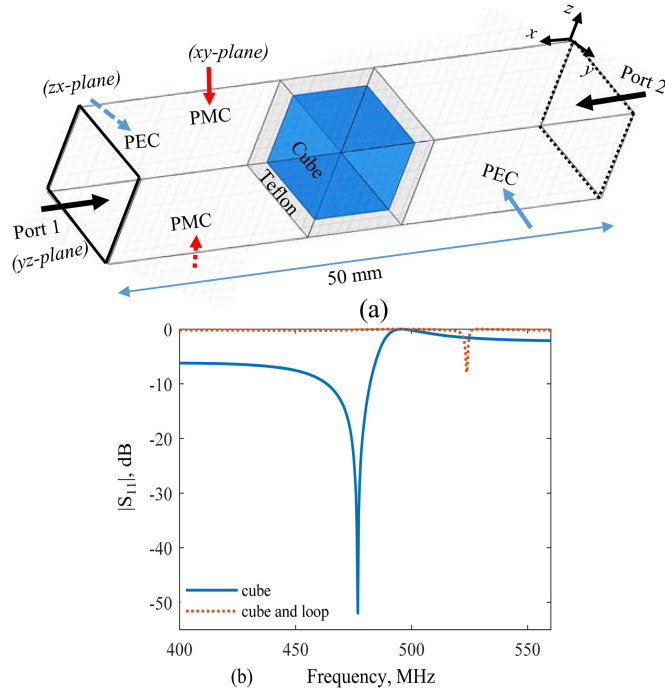


Fig. 2. (a) CHDR unit cell simulation setup. (b) Simulated reflection coefficient, $|S_{11}|$.

to (1). Therefore, the CHDR is supposed to be less sensitive to the polarization of the incident wave in the z -direction [see Fig. 1(a)]. As a result, the proposed WPT system shows superior performance due to receiver misalignment, which will be addressed in a later section.

2) HFSS Simulation: Initially, the cube size is chosen as $w = 15$ mm, having a permittivity $\epsilon_r = 1000$ and $\tan\delta = 0.00001$. This high-dielectric cube is surrounded by a low-dielectric ($\epsilon_r = 2.1$) Teflon substrate with a periodicity (or, lattice constant) $p = 19$ mm. The resonant frequency f of the lowest order modes for the above-mentioned CHDR resonators can be theoretically approximated based on the formulas given in (2), which gives us a resonant frequency of $f = 447.1$ MHz.

To verify the theoretical approximation, an Ansys HFSS model is established, as shown in Fig. 2(a). Using the finite-element solver of HFSS, the resonant frequency (f) was calculated under normal incidence. Taking advantage of the symmetry of the problem, the unit cell of the CHDR MTM was analyzed by applying two PMC and two PEC boundaries on the sides of the unit cell. The simulated resonant frequency was $f = 476.8$ MHz, which is very close to the calculated resonant frequency of $f = 447.1$ MHz according to the approximation in (2). The simulated reflection coefficient (S_{11}) is plotted, and this plot indicates that, if a small loop is placed in the vicinity of the unit cell, f shifts to a higher frequency, as depicted in Fig. 2(b).

B. CHDR MTM Characterization

In general, CHDR MTMs are composed of periodic arrangements of high-dielectric elements in a low-dielectric background. The periodicity (p) of the unit cell controls the

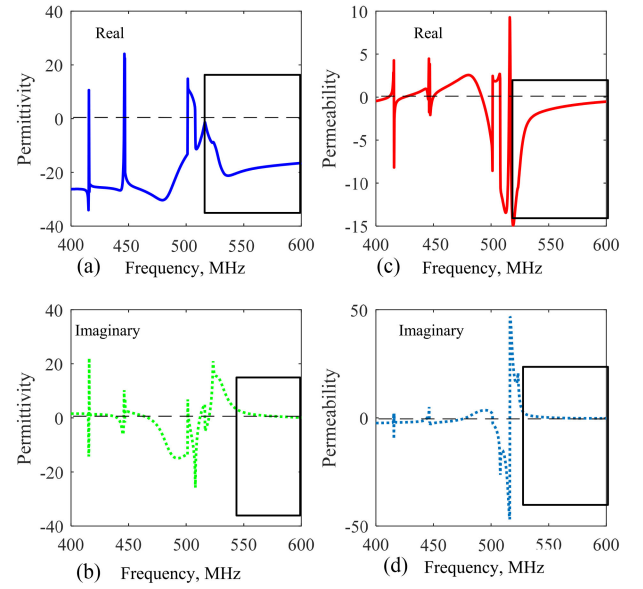


Fig. 3. Extracted parameter for the CHDR structure. (a) Real effective permittivity. (b) Imaginary effective permittivity. (c) Real effective permeability. (d) Imaginary effective permeability.

macroscopic resonance or the Bragg resonance, and the lattice resonance, whereas the microscopic resonance is due to the individual unit cell characteristics and is known as the Mie resonance. The combination of these two resonances gives rise to a negative refractive index [35]. According to Fig. 1, two CHDR structures with height $h = 36$ mm, $p = 19$ mm, and thickness $t = 19$ mm made of a 2×2 array of a high-dielectric ceramic cube enclosed in a low-dielectric (Teflon) background are considered. The MTM properties of the CHDR structure can be obtained by using a similar unit cell simulation setup [see Fig. 2(a)]; however, the unit cell should be replaced by the 2×2 CHDR array. The matrix elements S_{11} , S_{12} , S_{21} , and S_{22} are referred as the scattering parameters or the S -parameters. The parameters S_{11} and S_{22} have the meaning of reflection coefficients, and S_{12} and S_{21} define as the transmission coefficients. The S -parameters are related to both the refractive index (n) and the impedance (z). Therefore, extraction of parameters such as effective permittivity (ϵ_{eff}), effective permeability (μ_{eff}), and refractive index (n) are calculated based on the following equations [31]:

$$z = \pm \sqrt{\frac{(1 + S_{11})^2 - S_{21}^2}{(1 - S_{11})^2 - S_{21}^2}} \quad (3)$$

$$e^{\text{ink}_o d} = \frac{S_{21}}{1 - S_{11}[(z - 1)/(z + 1)]} \quad (4)$$

$$\epsilon_{\text{eff}} = n/z \quad \text{and} \quad \mu_{\text{eff}} = n \cdot z \quad (5)$$

where k_o and d denote the wave number and thickness of the MTM slab, respectively. The extracted real and imaginary parts of the effective permittivity and permeability are plotted in Fig. 3. A negative real part of either (or both) of these parameters enhances the evanescent wave amplification, whereas the imaginary part controls the loss associated with the system [14]. Fig. 3(a) and (c) represents the real part, whereas Fig. 3(b)

and (d) indicates the imaginary part of the effective permittivity and permeability, respectively. The region covered by the rectangular box is the negative refractive index region. In this portion of the plot, the real parts of both ϵ_{eff} and μ_{eff} become negative, and the imaginary parts are close to zero. Hence, the CHDR structure acts as an MTM with a negligible amount of loss.

C. MTM-Coupled WPT System Characterization

To realize the WPT system, the CHDR MTM is excited by using a simple square loop. The loop has dimensions of 30×30 mm with a thickness of 3 mm, as shown in Fig. 1. A feed/port with an impedance of 50Ω was placed in the loop, and a separation of $s = 4$ mm was selected between the loop and the CHDR structure. The distance (d) between the CHDR was 50 mm ($\approx 0.1\lambda$, and more than three times higher than the cube size, $w = 15$ mm). Under the simulation setup shown in Fig. 1, resonance occurs around $f = 560$ MHz, which lies in the negative refractive index zone (rectangular box portion) of Fig. 3. The reflection (S_{11}) and the transmission (S_{21}) coefficients are plotted in Fig. 4(a). A maximum WPT efficiency (η) of more than 91% was found according to Fig. 4(a), and η can be calculated based on the either of following equations [26]:

$$\eta = \frac{|S_{21}|^2}{1 - |S_{11}|^2} \quad (6)$$

$$\eta = |S_{21}|^2. \quad (7)$$

In general, the WPT efficiency based on (6) approximates the maximum achievable WPT efficiency, whereas (7) calculates the efficiency in a given situation. For a perfectly matched WPT system, (6) and (7) yield an almost identical maximum WPT efficiency, as visualized in Fig. 4(a).

According to the Mie theory under a proper excitation, a high-refractive-index dielectric exhibits very strong magnetic resonances. Owing to the high-dielectric contrast between free space and high dielectric, excitation of the CHDR resonator is expected to lead to strong localization of energy. To understand the above statement, the magnetic (H) and electric (E) field distributions are plotted in Fig. 4(b). As expected, the E and H fields are strongly confined in each cube inside the CHDR. The E field is swirling inside a CHDR cube, whereas the H field, which lies perpendicular to E , is penetrating inside and out of the CHDR structure. The field distributions correspond to the hybrid resonance mode resonating as a horizontal magnetic dipole (MD) [36], [37]. The hybrid resonance is one that is usually considered to originate from the very strong interactions between the elements in the unit cell [38]. In the plasmonic nanostructures, the horizontal MD mode is used to build efficient surface plasmon polariton couplers [36], whereas, in this paper, this mode has been applied to introduce an efficient WPT system. Fig. 4(c) represents the horizontal magnetic ($|H|$) dipole coupling for the proposed system; hence, this is referred to as the MTM-MD-coupled WPT system.

The mechanism of the proposed system is distinct from prior resonance-based wireless powering systems (or resonant system with an MTM slab) in that energy is localized in modes

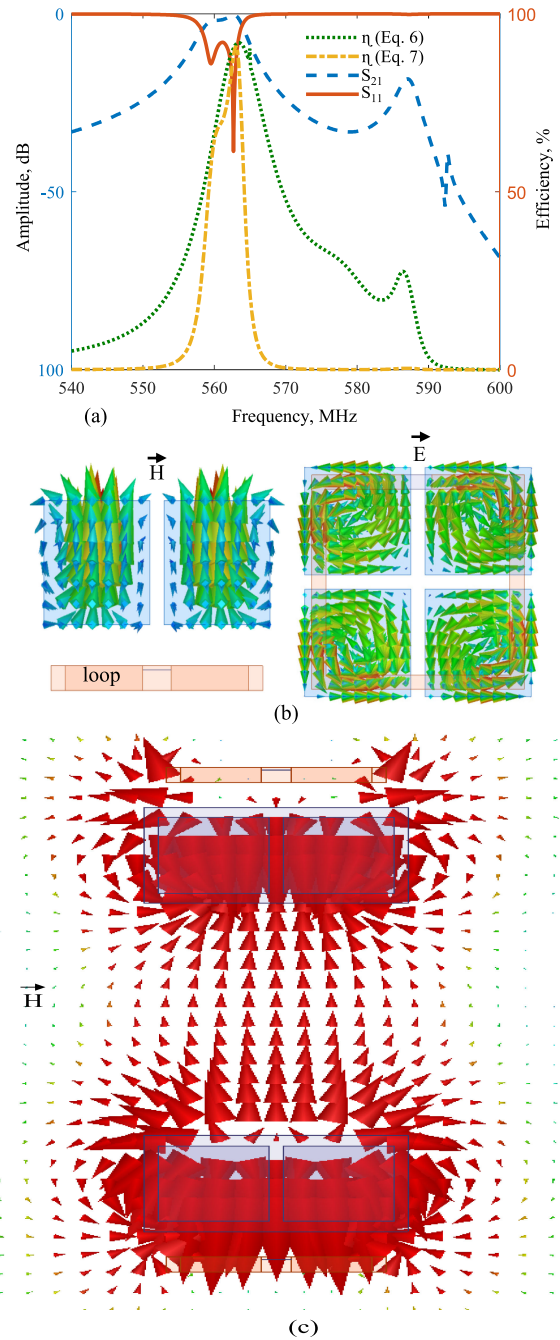


Fig. 4. (a) Characteristics of the proposed WPT system in terms of η , $|S_{11}|$, and $|S_{21}|$. (b) Magnetic ($|H|$) and electric ($|E|$) field distributions of the MTM-coupled WPT system. (c) Horizontal magnetic ($|H|$) dipole mode coupling for the proposed WPT system.

intrinsic in dielectric objects rather than engineered resonances in objects such as coils or antennas. As magnetic field coupling occurs between two CHDR MTMs, therefore, it is not necessary to design a sophisticated coil or antennas. We can use arbitrary nonresonant coils to excite or extract the power. The reason is that the magnetic field produced by source coil (see Fig. 1) can be drastically amplified by the transmitting MTM, which couples with the receiving MTM to form a whole system behaving similarly to the conventional four-coil system [7]. The

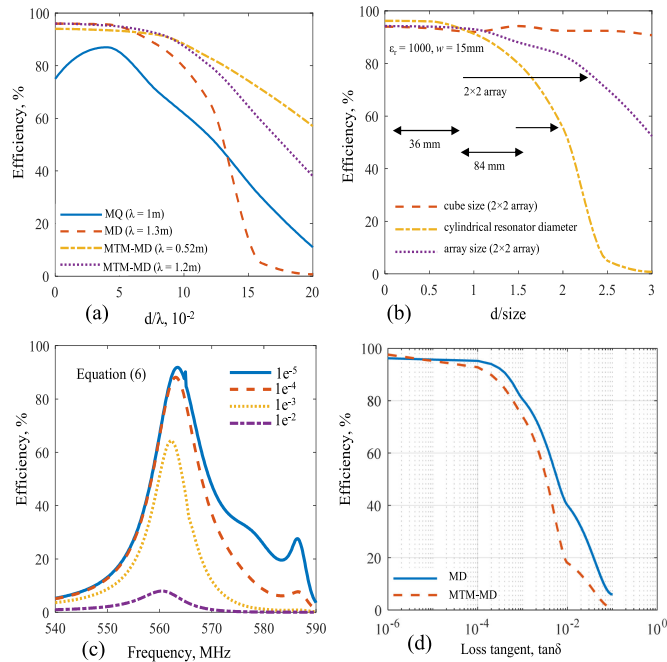


Fig. 5. Variations in η for different WPT systems when the distance is normalized by (a) operational wavelength, (b) array or dielectric size, (c) variations in efficiency due to the loss tangent, and (d) comparison between the MTM-MD mode and the MD mode in terms of $\tan\delta$ versus η .

role of magnetic MTMs is that they can largely weaken the fast divergence of the magnetic field lines in the nonresonant coils [13].

A comparison among different WPT techniques is plotted in Fig. 5. The distance dependencies of the efficiency (η) for MQ [25], MD (tuned) [26], and MTM-MD modes are compared based on (6) and are represented in Fig. 5(a). It should be noted that, to compare each WPT system working at different frequencies, the distance (d) was normalized by the corresponding wavelengths (λ). For simplicity, the loss tangent, $\tan\delta = 0.00001$, was considered for all cases. In order to make a fair comparison in terms of λ for both the MD and MQ modes, the cube size and permittivity of the MTM-MD mode (see Fig. 1) were adjusted to $w = 25$ mm and $p = 29$ mm, respectively, and $\varepsilon_r = 2000$. This setting gives an operational wavelength $\lambda \approx 1.22$ m for the MTM-MD mode. Fig. 5(a) indicates that all the WPT systems exhibit a very good efficiency (90%) at short distances. However, it is obvious from Fig. 5(a) that the proposed MTM-MD-based WPT system outperforms both the MD and MQ systems at long distances by a significant margin. Therefore, cascading small-sized multiple high-dielectric resonators, distributed with identical low-dielectric backgrounds, acts directly on the improvement of the evanescent wave coupling and decaying rate [39]. In addition, due to the “super-lens” effect ($\varepsilon_{\text{eff}} = -1$ or $\mu_{\text{eff}} = -1$) of the CHDR structure as revealed in Fig. 2, the range of WPT systems is also improved [21].

It is well known that the WPT efficiency in free space falls off rapidly when the operating distance (d) is larger than the largest size of the resonator [21]. Fig. 5(b) depicts the variations of η for different array and resonator sizes. The working WPT distance

(d) was normalized by the associated array or resonator size. Considering only the cube size ($w = 15$ mm) and periodicity $p = 19$ mm, no significant difference in efficiency was observed. Nonetheless, in comparison with the size (diameter $D = 84$ mm) of the cylindrical resonator proposed in [26], the improvement in WPT efficiency for the CHDR MTM is noteworthy. Furthermore, when the whole 2×2 CHDR array size (length or width = 36 mm) is considered, the proposed CHDR MTM array still performs much better than the cylindrical resonator for the same normalized distance. Numerically, an efficiency of more than 75% can be obtained when the separation between the CHDRs is twice as much as the array size under the matched condition, which, in contrast, indicates a more than 50% improvement in the WPT efficiency to the study in [26].

The WPT system efficiency was obtained at $\tan\delta = 0.00001$, which is difficult to achieve in reality. Hence, variations of efficiency in terms of the loss tangent is indicated in Fig. 5(c) and (d) for both the MD and MTM-MD modes. For simulation, the distance $d = 50$ mm and permittivity $\varepsilon_r = 1000$ were selected for each case. As expected from Fig. 5(c), a significant reduction in efficiency as well as in bandwidth (BW) occurs when the tangent loss increases. However, the drop of efficiency in the MTM-MD mode is higher than that in the MD mode according to Fig. 5(d), and the WPT efficiency is less than 20%, even when $\tan\delta = 0.01$ for the MTM-MD mode. This is due to fact that the CHDR structure in the MTM-MD mode contains multiple small resonators, and losses in each resonator become significant when $\tan\delta$ increases as compared to losses in a single dielectric resonator in the MD mode. Nonetheless, based on the high-dielectric material used in [26], which has a permittivity of 1000 and a loss tangent of $2.5e^{-4}$ at 1 MHz, the proposed MTM-coupled WPT system is expected to have a maximum efficiency of more than 80% for the proposed MTM coupled WPT system at a distance of 0.1λ .

III. PARAMETRIC STUDY

According to Fig. 1, there are several parameters that can influence the performance of the proposed WPT system. It is obvious from (1) that, by increasing the permittivity (ε_r) and/or cube size (w), the resonance frequency can be reduced. Therefore, in this section, the effect of other parameters such as periodicity (p), separation (s), variations in the MTM array, and transmitter/receiver size will be addressed. It is important to mention that the effect of changing different parameters of the CHDR structure on the MTM properties is discussed in [31]. This paper mainly focuses on the MTM-coupled WPT system; therefore, how the aforementioned parameters affect the whole WPT system (e.g., S_{11} and/or η) will be investigated.

A. Variation in Periodicity (p) and Separation (s)

Fig. 6(a) and (b) represents the variations in the WPT efficiency due to changes in periodicity (p) and separation (s), and the corresponding simulation parameters are indicated in each plot. According to Fig. 6(a), when the periodicity (p) increases, the resonant frequency of the proposed WPT system shifts to a lower frequency, and the maximum η for each case remains

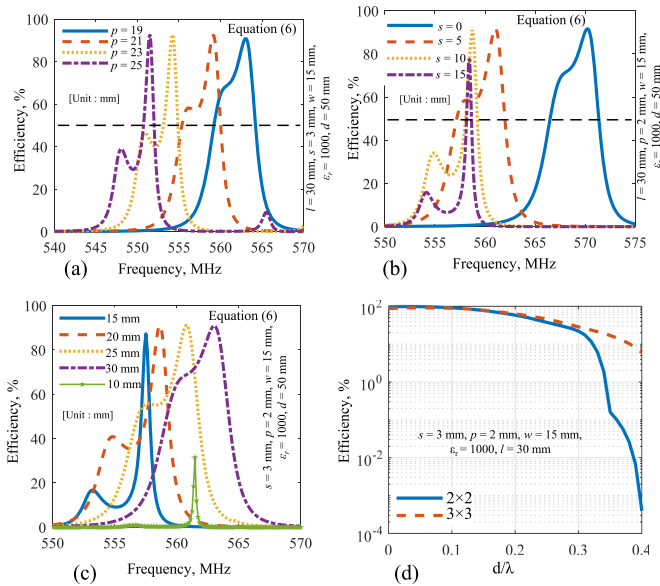


Fig. 6. Parametric studies and variations in (a) periodicity, p , (b) separation, s , (c) transmitter and receiver size, l , and (d) number of arrays.

almost the same. However, a reduction in the WPT efficiency BW was observed with increments in p . This reduction in the BW is indicated by drawing a black dashed line along the x -axis at 50% WPT efficiency. Similar results were found due to a change in periodicity of the CHDR structure by *Kim et al.* Furthermore, the separation (s) between the transmitter/receiver and the CHDR also influences the resonant frequency and the BW. Fig. 6(b) indicates that the resonant frequency of the proposed WPT system can be tuned by adjusting the distance (s) [26]. It is observed that, depending on the transmitter/receiver size (l), for each distance (d), there is an optimum separation (s), at which η is the maximum. Furthermore, the separation (s) is increased with an increasing distance (d), and the value of s should not be more than the resonator size (w) at short distances ($\leq 0.1\lambda$).

B. Variation in Transmitter/Receiver Size and Number of Arrays

It is important to minimize the transmitter/receiver size for various applications. As an example, nowadays, WPT in implantable devices is becoming more popular, which requires a smaller transmitter or receiver size. Variation in the transmitter and receiver size (length) as well as their corresponding efficiency is plotted in Fig. 6(c). It is interesting to observe that there is almost no change in the maximum efficiency ($\approx 90\%$) when both the transmitter and receiver lengths are gradually reduced from 30 to 15 mm. In addition, reduction in length of the excitation element also reduces the BW as well as the resonant frequency. However, a notable alteration in resonant properties and reduction in efficiency were found as soon as the length decreases below 15 mm, which happens to be equal to the cube resonator length, $w = 15$ mm. Hence, the resonator size plays an important role in determining the maximum separation distance

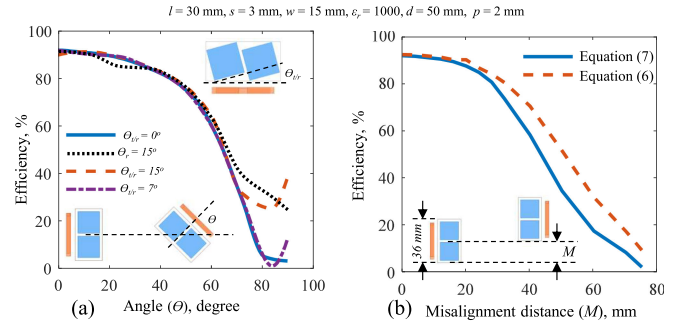


Fig. 7. Parametric studies and variations in efficiency of the proposed WPT system due to (a) misorientation, θ and (b) displacement, M .

(s) and the minimum transmitter/receiver size (l) to obtain the maximum WPT output for the proposed system. Another necessary parametric study is the number of MTM arrays, as it significantly affects the power transfer distance. A comparison between 2×2 and 3×3 arrays is revealed in Fig. 6(d). According to this plot, the 3×3 array shows a significant improvement in η beyond the 0.3λ transfer distance as compared to the 2×2 array. This finding is identical to the study in [29]. As a consequence, the number of MTM arrays can be adjusted in accordance with the required transfer distance.

C. Receiver Misalignment

An efficient WPT system should be able to transfer power even if a misalignment exists between the transmitter and/or the receiver end. Depending on the misalignment susceptibility, the overall proficiency of a WPT system can be approximated. Here, the misalignment from the receiver end is considered. In general, two types of misplacement can occur, one is due to misorientation (θ) and the other is due to displacement (M), as visualized in Fig. 7(a) and (b), respectively. According to Fig. 7(a), the maximum WPT efficiency of the proposed system remains at more than 50% at $\theta = 60^\circ$ and decreases quickly to 3% for complete misorientation at $\theta = 90^\circ$. However, a significant improvement in η was found when the MTM cubes are rotated along with θ . At first, only the receiver end cubes are rotated at an angle, $\theta_r = 15^\circ$, which gives a noteworthy enhancement in efficiency when θ is more than 80° . In addition, a rotation in the MTM cubes for both the transmitter and receiver ends ($\theta_{t/r}$) results in a remarkable boost in efficiency at $\theta = 90^\circ$. Based on the simulated results, the maximum WPT efficiency can be more than 35% at $\theta = 90^\circ$ for $\theta_{t/r} = 15^\circ$. As a consequence, the cube orientation ($\theta_{t/r}$) can be adjusted to obtain a reasonable amount of power transfer efficiency supposing a completely misoriented receiver end. Fig. 7(b) shows the change in η due to displacement M . It is interesting to see that, at a distance $d = 50$ mm, when the receiver end is entirely out of sight from the transmitter end (i.e., at $M = 36$ mm), this WPT system still maintains more than 50% efficiency, which implies a great susceptibility of the proposed WPT system to misalignments.

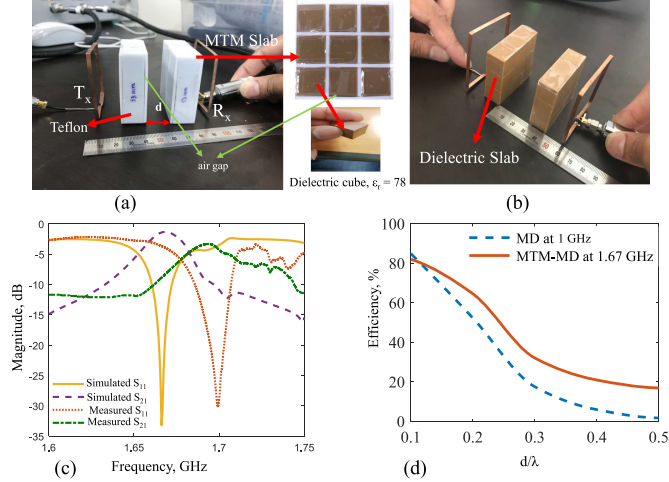


Fig. 8. (a) Photograph of the proposed MTM-MD WPT system along with the MTM slab. (b) Photograph of the MD-based WPT system. (c) Simulated and measured S_{11} and S_{21} for the proposed WPT system at 0.1λ . (d) Variation in efficiency due to the working distance for the MTM-MD and MD-based WPT systems.

IV. EXPERIMENTAL VERIFICATION OF THE PROPOSED WPT SYSTEM

To validate the proposed method, the CHDR cube material was chosen as microwave ceramic samples of EXXELIA TEMEX E5080 along with a cube size $w = 15$ mm. Unfortunately, this ceramic only has a permittivity $\epsilon_r = 78$, permeability $\mu_r = 1$, and a loss tangent $\tan\delta = 0.0004$. As a result, the resonant frequency was scaled up to higher frequencies (lower gigahertz range). Fig. 8(a) shows a photograph of the experimental setup along with MTM slabs. It should be noted that at high frequency, loss increases and the evanescent wave decays more rapidly. Hence, instead of using a 2×2 array, a 3×3 array is used, and the size of the transmitter (T_x) and receiver (R_x) loop also increased accordingly to achieve the proper S_{11} . For measurements, two identical 3×3 CHDR MTMs having dimensions of $53 \text{ mm} \times 53 \text{ mm} \times 19 \text{ mm}$ are separated by a distance d and excited by two similar rectangular loops of dimensions $50 \text{ mm} \times 50 \text{ mm}$. The thickness of the loop was 0.5 mm. The periodicity p and the separation s were selected as 19 and 15 mm, respectively. In addition, to make a fair comparison between the recently introduced MD-based WPT systems and the proposed WPT system, the MD WPT system [26] was created by combining all the available cubes to act as a dielectric slab, as shown in Fig. 8(b). From simulation, the resonant frequencies for the MD and MTM-MD modes were found as 1 and 1.67 GHz, respectively. The simulated and measured reflection (S_{11}) and transmission coefficients (S_{21}) for the MTM-MD WPT system are plotted in Fig. 8(c). The measured resonance frequency was found at 1.7 GHz, and the maximum S_{21} measured as -2.43 dB as compared to the simulated S_{21} of -1.3 dB at $d = 20$ mm (0.1λ). The deviation between the simulated and measured results mainly occurs due to the presence of a visible air gap between cubes and Teflon. This air gap influences the performance of the MTM slab and coupling. The mismatch between the T_x and R_x loop also affected the

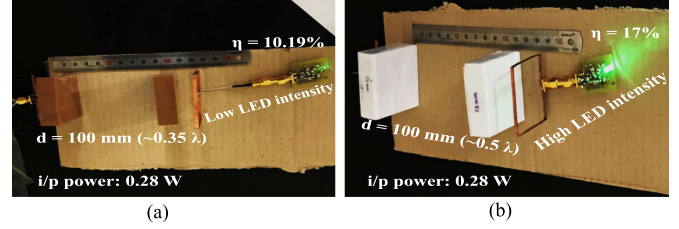


Fig. 9. Demonstration of the long-range power transfer capability for (a) MD [26] and (b) MTM-MD WPT systems.

measured results. Considering all these experimental limitations, the measured results remain almost identical to the simulated results. For $\epsilon_r = 78$, efficiency versus distance variations is plotted in Fig. 8(d). The efficiency was calculated based on (5), and the working WPT distance (d) was normalized by the associated wavelength (λ). The results in Fig. 8(d) matched the results predicted in Fig. 5(a), where both WPT systems achieve 80% efficiency within a short distance. However, for the same normalized distance, the MTM-MD-based WPT system achieves a higher efficiency at long distances (0.3λ or more) as compared to the MD-based WPT system. To illustrate this, a green LED is connected *via* a rectifier to the receiver end for both cases, and a working WPT distance was chosen as $d = 100$ mm.

Fig. 9 demonstrates and compares the performance of the MTM-MD and MD WPT systems at $d = 100$ mm. For the same power input from the power amplifier, the intensity of the LED for the proposed WPT system is higher than the MD-based WPT system. The performance of both systems in terms of efficiency and operational wavelength is also indicated in Fig. 9. It is obvious from this demonstration that the proposed WPT system is highly efficient at short distances and can be applied for long-range power transfer. Furthermore, a comparison table among previous studies and the proposed WPT system is shown in Table I. This comparison testifies that the MTM-MD-based WPT systems are not only superior in terms of η improvement and transfer distance, but the proposed method also requires lower transmitter and receiver sizes, thus establishing the idea of an MTM-coupled, highly efficient, miniaturized, and long-range WPT system.

For a versatile WPT system, misalignment and misorientation of T_x/R_x should also be evaluated. The effect of receiver misalignment on the WPT efficiency is addressed in detail in Section III. Experimentally, a demonstration of misalignment was examined by introducing displacement M in the R_x end, as shown in Fig. 10. The displacement M is selected as 53 mm. The distance d is chosen as 130 mm, and more than 5% efficiency was achieved for the MTM-MD case at a distance of 0.65λ even when the R_x end is completely out of sight from the T_x end. However, the received η reduced to 1.4% without the MTM coupling. By doubling the input power compared to Fig. 9, the received power without MTM not enough to turn ON the LED, as indicated in Fig. 10(a). In contrast, by simply placing the MTMs for the same input power, the LED shines brightly, as revealed in Fig. 10(b). This illustration provides insight into the power transfer capability of the proposed WPT system for misalignments.

TABLE I
COMPARISON OF THE PROPOSED WPT SYSTEM WITH PREVIOUS WORKS

Ref.	Operating Frequency	Tx Size	Rx Size	Transfer Distance (d)	MTM or Dielectric Size	S_{21} Improvement (dB)	η Improvement
[7]	10 MHz	$\pi \times 60 \times 60 \text{ cm}^2$	$\pi \times 60 \times 60 \text{ cm}^2$	200 cm (0.06 λ)	–	–	45%
[13]	23.4 MHz	$7.8 \times 7.8 \text{ cm}^2$	$7.8 \times 7.8 \text{ cm}^2$	7 cm (0.0055 λ)	$7.8 \times 7.8 \text{ cm}^2$	–	5% to 40%
[17]	27 MHz	$\pi \times 2.5 \times 2.5 \text{ cm}^2$	$\pi \times 1.8 \times 1.8 \text{ cm}^2$	5 cm (0.0045 λ)	$6.9 \times 6.9 \text{ cm}^2$	-9.47 to -7.4	11.3% to 18.2%
[18]	6.78 MHz	$15 \times 15 \text{ cm}^2$	$15 \times 15 \text{ cm}^2$	30 cm (0.0068 λ)	$18.6 \times 18.6 \text{ cm}^2$	-23 to -18.9	0.5% to 1.3%
[28]	27.1 MHz	$\pi \times 20 \times 20 \text{ cm}^2$	$\pi \times 20 \times 20 \text{ cm}^2$	50 cm (0.045 λ)	$58.5 \times 58.5 \text{ cm}^2$	-7.68 to -3.28	17% to 47%
[29]	6.3 MHz	$\pi \times 25 \times 25 \text{ cm}^2$	$\pi \times 25 \times 25 \text{ cm}^2$	100 cm (0.02 λ)	$70 \times 70 \text{ cm}^2$	-7 to -2.65	19.9% to 54.3%
[26]	232 MHz	$\pi \times 3.6 \times 3.6 \text{ cm}^2$	$\pi \times 3.6 \times 3.6 \text{ cm}^2$	16 cm (0.124 λ)	$\pi \times 3.7 \times 3.7 \text{ cm}^2$	–	50%
[This Work: $\epsilon_r = 1000$ (Simulation)]	560 MHz	$3 \times 3 \text{ cm}^2$	$3 \times 3 \text{ cm}^2$	10 cm (0.19 λ)	$3.6 \times 3.6 \text{ cm}^2$	–	58.5% (Eq. 5)
[This Work: $\epsilon_r = 78$ (Measured)]	1.7 GHz	$5 \times 5 \text{ cm}^2$	$5 \times 5 \text{ cm}^2$	3.6 cm (0.2 λ)	$5.3 \times 5.3 \text{ cm}^2$	–	52% (Eq. 5)

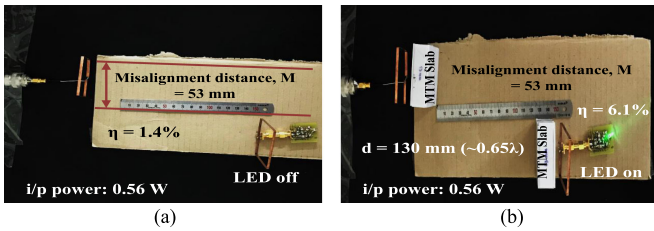


Fig. 10. Variation in efficiency due to misalignment. (a) Traditional WPT system. (b) MTM-MD-based WPT system.

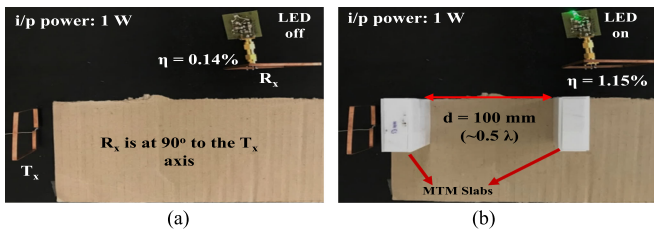


Fig. 11. Demonstration of WPT efficiency considering the worst-case scenario of “s.” (a) Traditional WPT. (b) MTM-MD WPT systems.

In the MTM-MD-based WPT system, the large separation (s) also signifies that magnetic field coupling occurs between the two MTM resonators; therefore, T_x and R_x can be moved independently. This phenomenon is displayed in Fig. 11, where R_x is placed at the worst position possible, with complete displacement to the T_x -axis and rotated by 90° . For $d = 100 \text{ mm}$ (0.5λ), traditional WPT gives a negligible transfer efficiency of 0.14% as opposed to the 1.15% for the proposed WPT system. These results are also reflected by Fig. 11(a) and (b) for the power input of 1 W. This separation “ s ” feature enables future studies, where there will be no need to place the devices (R_x end) on a charging pad for wireless charging. Instead, we will be able to establish truly wireless charging as long as the devices remain in the MTM-coupled region.

The SAR still remains a concern with the WPT system [40], [41]. If any human tissue/implantable device lies in the middle

of T_x and the R_x , it may be exposed to the electromagnetic fields produced by the WPT system, thus causing tissue heating or implant damage. This exposure or SAR limit is defined by the ICNIRP guidelines [41], which recommend that whole-body SAR does not exceed 0.08 W/kg and 10-g SAR does not exceed 2 W/kg for the head and the trunk and 4 W/kg for limbs. In this paper, the separation (s) between the T_x/R_x and the MTM slab (see Fig. 1) plays an important role to reduce the SAR. The parameter “ s ” can be adjusted for tuning the WPT system and to optimize the WPT efficiency, as discussed in Section III-A. It is also mentioned that for optimizing efficiency, “ s ” can be increased with an increasing distance d . This situation has many advantages. In one case, the proposed method can reduce the SAR as well as increase the efficiency compared to the most commonly used inductive/resonant coupling. An HFSS simulation illustration of the SAR is shown in Fig. 12. For the simulation setup, a cylindrical skin phantom ($\epsilon_r = 39.2$ and $\sigma = 1.11$ at 1.7 GHz) of radius 3 cm and height 5.3 cm is placed in between the transmitter and receiver side, and the distance d was chosen as 72 mm. Two similar rectangular loops of dimension $50 \times 50 \text{ mm}$ were considered as T_x and R_x . For simplicity, simulated 1-g SAR was normalized to 1 W/kg. As visualized in Fig. 12(b), in traditional inductive coupling if the exciting element (i.e., T_x) lies very close to human tissue, it introduces a local hot spot inside the tissue, as opposed to the MTM-coupled WPT system in Fig. 12(a). In addition, it is important to note that the simulated received efficiency is almost four times higher in the case of the proposed WPT system as compared to the traditional WPT system, even when the T_x and the R_x are more than 20 cm apart from each other. Measurement validation is carried out by placing a simple cup of fresh water as a phantom in the middle of T_x and R_x separated by 70 mm, as indicated in Fig. 12(c). From Fig. 12(c) and (d), it can be confirmed that, for the same power input of 0.7 W, the MTM-MD-based WPT system offers higher η as compared to the traditional WPT system, as indicated by the LED. Due to low SAR and high η in the MTM-MD WPT system, the input power can also be increased to reach the SAR safety limit when more power is required by a system.

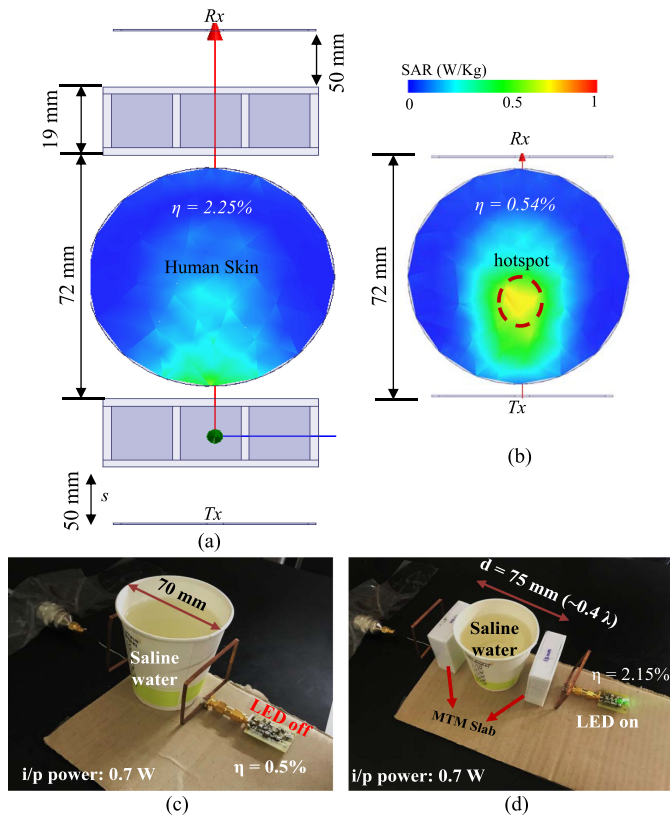


Fig. 12. Normalized 1-g local SAR calculation in human skin tissue for (a) the MTM-MD-based WPT system and (b) the traditional inductive-coupling-based WPT system. Measurements in a simple cup containing fresh water for (c) the traditional WPT system. (d) Proposed MTM-MD system.

V. CONCLUSION

In this paper, a WPT system referred to as “MTM-MD,” based on two CHDR MTMs, which are excited by two similar non-resonant oops, was explored. The CHDR MTM is composed of an array of cubic high dielectrics arranged in a low-dielectric background. From HFSS simulation, it is observed that this WPT system introduces a horizontal MD between the CHDR MTMs and achieves more than 80% efficiency at short distances and 50% efficiency at a distance of 0.2λ . The proposed WPT system requires a smaller footprint for higher efficiency compared to previous studies, and the transmitter and receiver sizes should not be lower than the CHDR’s cube size for a reasonable WPT efficiency. It is also found that a larger CHDR array helps improve the range of the WPT system. For measurements, the CHDR MTMs were designed by considering microwave ceramic samples of EXXELIA TEMEX E5080 for high-dielectric cubes, and Teflon was selected as a low-dielectric background. Experimental comparison between the most recent high-dielectric-coupled WPT system and the proposed system was also carried out to demonstrate the long-range power transfer capability. The versatility of the system was also discussed by considering the receiver misalignment. We found that the suggested WPT system can withstand receiver displacement from the transmitter axis, as well as the orientation of the cubes inside the CHDR MTM can be adjusted for misorientation while

maintaining an efficient WPT system. Furthermore, the MTM-MD WPT system performed superiorly in the presence of a tissue like material in terms of the SAR and efficiency as compared to the traditional WPT system. Due to the heterogeneous nature of the human tissues, it is expected that the proposed dielectric-based method will only expose or stimulate the desired part without affecting the surrounding media. Hence, the proposed concept can be explored to power up a tiny medical device or to give tissue-specific heating for hyperthermia without affecting the surrounding tissues and so on.

REFERENCES

- [1] S. Y. R. Hui, W. Zhong, and C. K. Lee, “A critical review of recent progress in mid-range wireless power transfer,” *IEEE Trans. Power Electron.*, vol. 29, no. 9, pp. 4500–4511, Sep. 2014, doi: [10.1109/TPEL.2013.2249670](https://doi.org/10.1109/TPEL.2013.2249670).
- [2] S. Y. Hui, “Planar wireless charging technology for portable electronic products and Qi,” *Proc. IEEE*, vol. 101, no. 6, pp. 1290–1301, Jun. 2013, doi: [10.1109/JPROC.2013.2246531](https://doi.org/10.1109/JPROC.2013.2246531).
- [3] J. S. Ho *et al.*, “Wireless power transfer to deep-tissue microimplants,” *Proc. Nat. Acad. Sci. U.S.A.*, vol. 111, no. 22, pp. 7974–7979, Jun. 2014, doi: [10.1073/pnas.1403002111](https://doi.org/10.1073/pnas.1403002111).
- [4] C. C. Mi, G. Bujja, S. Y. Choi, and C. T. Rim, “Modern advances in wireless power transfer systems for roadway powered electric vehicles,” *IEEE Trans. Ind. Electron.*, vol. 63, no. 10, pp. 6533–6545, Oct. 2016, doi: [10.1109/TIE.2016.2574993](https://doi.org/10.1109/TIE.2016.2574993).
- [5] J. Shin *et al.*, “Design and implementation of shaped magnetic-resonance-based wireless power transfer system for roadway-powered moving electric vehicles,” *IEEE Trans. Ind. Electron.*, vol. 61, no. 3, pp. 1179–1192, Mar. 2014, doi: [10.1109/TIE.2013.2258294](https://doi.org/10.1109/TIE.2013.2258294).
- [6] N. Tesla, “Apparatus for transmitting electrical energy,” U.S. Patent 1 119 732, Dec. 1, 1914. [Online]. Available: <https://www.google.com/patents/US1119732>
- [7] A. Kurs, A. Karalis, R. Moffatt, J. D. Joannopoulos, P. Fisher, and M. Soljacic, “Wireless power transfer via strongly coupled magnetic resonances,” *Science*, vol. 317, pp. 83–86, Jul. 2007, doi: [10.1126/science.1143254](https://doi.org/10.1126/science.1143254).
- [8] J. Zhang, X. Yuan, C. Wang, and Y. He, “Comparative analysis of two-coil and three-coil structures for wireless power transfer,” *IEEE Trans. Power Electron.*, vol. 32, no. 1, pp. 341–352, Jan. 2017, doi: [10.1109/TPEL.2016.2526780](https://doi.org/10.1109/TPEL.2016.2526780).
- [9] A. P. Sample, D. T. Meyer, and J. R. Smith, “Analysis, experimental results, and range adaptation of magnetically coupled resonators for wireless power transfer,” *IEEE Trans. Ind. Electron.*, vol. 58, no. 2, pp. 544–554, Feb. 2011, doi: [10.1109/TIE.2010.2046002](https://doi.org/10.1109/TIE.2010.2046002).
- [10] B. L. Cannon, J. F. Hoburg, and D. D. Stancil, “Magnetic resonant coupling as a potential means for wireless power transfer to multiple small receivers,” *IEEE Trans. Power Electron.*, vol. 24, no. 7, pp. 1819–1825, Jul. 2009, doi: [10.1109/TPEL.2009.2017195](https://doi.org/10.1109/TPEL.2009.2017195).
- [11] W. Zhong and S. Y. R. Hui, “Charging time control of wireless power transfer systems without using mutual coupling information and wireless communication system,” *IEEE Trans. Ind. Electron.*, vol. 64, no. 1, pp. 228–235, Jan. 2017, doi: [10.1109/TIE.2016.2598725](https://doi.org/10.1109/TIE.2016.2598725).
- [12] N. L. Zhen, R. A. Chinga, and R. Tseng, “Design and test of a high-power high-efficiency loosely coupled planar wireless power transfer system,” *IEEE Trans. Ind. Electron.*, vol. 56, no. 5, pp. 1801–1812, May 2009, doi: [10.1109/TIE.2008.2010110](https://doi.org/10.1109/TIE.2008.2010110).
- [13] Q. Wu *et al.*, “Wireless power transfer based on magnetic metamaterials consisting of assembled ultra-subwavelength meta-atoms,” *Europhys. Lett.*, vol. 109, no. 6, Mar. 2015, Art. no. 68005, doi: [10.1209/0295-5075/109/68005](https://doi.org/10.1209/0295-5075/109/68005).
- [14] L. Li, H. Liu, H. Zhang, and W. Xue, “Efficient wireless power transfer system integrating with metasurface for biological applications,” *IEEE Trans. Ind. Electron.*, vol. 65, no. 4, pp. 3230–3239, Apr. 2018, doi: [10.1109/TIE.2017.2756580](https://doi.org/10.1109/TIE.2017.2756580).
- [15] Y. J. Kim, D. Ha, W. J. Chappell, and P. P. Irazoqui, “Selective wireless power transfer for smart power distribution in a miniature-sized multiple receiver system,” *IEEE Trans. Ind. Electron.*, vol. 63, no. 3, pp. 1853–1862, Mar. 2016, doi: [10.1109/TIE.2015.2493142](https://doi.org/10.1109/TIE.2015.2493142).
- [16] M. Zargham and P. G. Gulak, “Maximum achievable efficiency in nearfield coupled power-transfer systems,” *IEEE Trans. Biomed. Circuits Syst.*, vol. 6, no. 3, pp. 228–245, Jun. 2012, doi: [10.1109/TBCAS.2011.2174794](https://doi.org/10.1109/TBCAS.2011.2174794).

- [17] A. Rajagopalan, A. K. RamRakhyani, D. Schurig, and G. Lazzi, "Improving power transfer efficiency of a short-range telemetry system using compact metamaterials," *IEEE Trans. Microw. Theory Techn.*, vol. 62, no. 4, pp. 947–955, Apr. 2014, doi: [10.1109/TMTT.2014.2304927](https://doi.org/10.1109/TMTT.2014.2304927).
- [18] Y. Cho *et al.*, "Thin PCB-type metamaterials for improved efficiency and reduced EMF Leakage in wireless power transfer systems," *IEEE Trans. Microw. Theory Techn.*, vol. 64, no. 2, pp. 353–364, Feb. 2016, doi: [10.1109/TMTT.2015.2514090](https://doi.org/10.1109/TMTT.2015.2514090).
- [19] D. R. Agrawal *et al.*, "Conformal phased surfaces for wireless powering of bioelectronic microdevices," *Nature Biomed. Eng.*, vol. 1, Mar. 2017, Art. no. 0043, doi: [10.1038/s41551-017-0043](https://doi.org/10.1038/s41551-017-0043).
- [20] S. Du *et al.*, "Wireless power transfer using oscillating magnets," *IEEE Trans. Ind. Electron.*, vol. 65, no. 8, pp. 6259–6269, Aug. 2018, doi: [10.1109/TIE.2017.2786289](https://doi.org/10.1109/TIE.2017.2786289).
- [21] G. Lipworth *et al.*, "Magnetic metamaterial superlens for increased range wireless power transfer," *Sci. Rep.*, vol. 4, Jan. 2014, Art. no. 3642, doi: [10.1038/srep03642](https://doi.org/10.1038/srep03642).
- [22] D. Liu, H. Hu, and S. V. Georgakopoulos, "Misalignment sensitivity of strongly coupled wireless power transfer systems," *IEEE Trans. Power Electron.*, vol. 32, no. 7, pp. 5509–5519, Jul. 2017, doi: [10.1109/TPEL.2016.2605698](https://doi.org/10.1109/TPEL.2016.2605698).
- [23] J. P. K. Sampath, A. Alphones, and D. M. Vilathgamuwa, "Figure of merit for the optimization of wireless power transfer system against misalignment tolerance," *IEEE Trans. Power Electron.*, vol. 32, no. 6, pp. 4359–4369, Jun. 2017, doi: [10.1109/TPEL.2016.2601939](https://doi.org/10.1109/TPEL.2016.2601939).
- [24] N. H. Van and C. Seo, "Analytical and experimental investigations of omnidirectional wireless power transfer using a cubic transmitter," *IEEE Trans. Ind. Electron.*, vol. 65, no. 2, pp. 1358–1366, Feb. 2018, doi: [10.1109/TIE.2017.2733470](https://doi.org/10.1109/TIE.2017.2733470).
- [25] M. Song, I. Iorsh, P. Kapitanova, E. Nenasheva, and P. Belov, "Wireless power transfer based on magnetic quadrupole coupling in dielectric resonators," *Appl. Phys. Lett.*, vol. 108, Jan. 2016, Art. no. 023902, doi: [10.1063/1.4939789](https://doi.org/10.1063/1.4939789).
- [26] M. Song, P. Belov, and P. Kapitanova, "Wireless power transfer based on dielectric resonators with colossal permittivity," *Appl. Phys. Lett.*, vol. 109, Dec. 2016, Art. no. 223902, doi: [10.1063/1.4971185](https://doi.org/10.1063/1.4971185).
- [27] M. C. K. Wiltshire, J. B. Pendry, I. R. Young, D. J. Larkman, D. J. Gilderdale, and J. V. Hajnal, "Microstructured magnetic materials for RF flux guides in magnetic resonance imaging," *Science*, vol. 291, no. 5505, pp. 849–851, Feb. 2001, doi: [10.1126/science.291.5505.849](https://doi.org/10.1126/science.291.5505.849).
- [28] B. Wang, K. H. Teo, T. Nishino, W. Yerazunis, J. Barnwell, and J. Zhang, "Experiments on wireless power transfer with metamaterials," *Appl. Phys. Lett.*, vol. 98, Jun. 2011, Art. no. 254101, doi: [10.1063/1.3601927](https://doi.org/10.1063/1.3601927).
- [29] A. L. A. K. Ranaweera, T. P. Duong, and J. W. Lee, "Experimental investigation of compact metamaterial for high efficiency mid-range wireless power transfer applications," *J. Appl. Phys.*, vol. 116, Jul. 2014, Art. no. 043914, doi: [10.1063/1.4891715](https://doi.org/10.1063/1.4891715).
- [30] D. R. Smith, J. B. Pendry, and M. C. K. Wiltshire, "Metamaterials and negative refractive index," *Science*, vol. 305, no. 5685, pp. 788–792, Aug. 2004, doi: [10.1126/science.1096796](https://doi.org/10.1126/science.1096796).
- [31] J. Kim and A. Gopinath, "Simulation of a metamaterial containing cubic high dielectric resonators," *Phys. Rev. B*, vol. 76, Sep. 2007, Art. no. 115126, doi: [10.1103/PhysRevB.76.115126](https://doi.org/10.1103/PhysRevB.76.115126).
- [32] S. O'Brien and J. B. Pendry, "Photonic band-gap effects and magnetic activity in dielectric composites," *J. Phys.: Condens. Matter*, vol. 14, pp. 4035–4044, Apr. 2002, doi: [JPhysCM/14/4035](https://doi.org/10.1088/0953-2084/14/4035).
- [33] E. Cubukcu, K. Aydin, E. Ozbay, S. Foteinopoulou, and C. M. Soukoulis, "Electromagnetic waves: Negative refraction by photonic crystals," *Nature*, vol. 423, pp. 604–605, Jun. 2003, doi: [10.1038/423604b](https://doi.org/10.1038/423604b).
- [34] K. Agarwal *et al.*, "Three-dimensionally coupled THz octagrams as isotropic metamaterials," *ACS Photon.*, vol. 4, pp. 2436–2445, Sep. 2017, doi: [10.1021/acsp Photonics.7b00617](https://doi.org/10.1021/acsp Photonics.7b00617).
- [35] R. Das and H. Yoo, "Application of a compact electromagnetic bandgap array in a phone case for suppression of mobile phone radiation exposure," *IEEE Trans. Microw. Theory Techn.*, vol. 66, no. 5, pp. 2363–2372, May 2018, doi: [10.1109/TMTT.2017.2786287](https://doi.org/10.1109/TMTT.2017.2786287).
- [36] C. Zou, W. Withayachumnankul, M. Bhaskaran, S. Sriram, and C. Fumeaux, "Dielectric resonator nanoantennas: A review of the theoretical background, design examples, prospects, and challenges," *IEEE Antennas Propag. Mag.*, vol. 59, no. 6, pp. 30–42, Dec. 2017, doi: [10.1109/MAP.2017.2752638](https://doi.org/10.1109/MAP.2017.2752638).
- [37] A. Petosa, *Dielectric Resonator Antenna Handbook*. Norwood, MA, USA: Artech House, 1997.
- [38] A. N. Serdyukov, I. V. Semchenko, S. A. Tretyakov, and A. Sihvola, *Electromagnetics of Bi-Anisotropic Materials: Theory and Application*. Amsterdam, The Netherlands: Gordon and Breach Science, 2001.
- [39] R. Castro-Beltran, N. Huby, G. Loas, H. Lhermite, D. Pluchon, and B. Beche, "Improvement of efficient coupling and optical resonances by using taper-waveguides coupled to cascade of UV210 polymer microresonators," *J. Micromech. Microeng.*, vol. 24, no. 12, Nov. 2014, Art. no. 125006, doi: [10.1088/0960-1317/24/12/125006](https://doi.org/10.1088/0960-1317/24/12/125006).
- [40] R. L. McIntosh, V. Anderson, R. J. McKenzie, "A numerical evaluation of SAR distribution and temperature changes around a metallic plate in the head of a RF exposed worker," *Bioelectromagnetics*, vol. 26, no. 5, pp. 377–388, May 2005, doi: [10.1002/bem.20112](https://doi.org/10.1002/bem.20112).
- [41] International Commission on Non-Ionizing Radiation Protection, "Guidelines for limiting exposure to time-varying electric, magnetic, and electromagnetic fields (up to 300 GHz)," *Health Phys.*, vol. 75, no. 4, pp. 494–522, Oct. 1998. [Online]. Available: <https://www.icnirp.org/cms/upload/publications/ICNIRPemfgdl.pdf>



Rupam Das received the B.Sc. degree in electrical and electronics engineering from the Chittagong University of Engineering and Technology, Chittagong, Bangladesh, in 2011, and the M.Sc. and Ph.D. degrees in biomedical engineering from the University of Ulsan, Ulsan, South Korea, in 2013 and 2017, respectively.

From 2017 to 2018 he was a Postdoctoral Associate of Biomedical Engineering with the University of Ulsan and Hanyang University, Seoul, South Korea, respectively. He is currently a Research Associate with the Department of Engineering at the University of Glasgow, Glasgow, Scotland, U.K. His current research interests include implantable antennas and devices, wireless power transfer, metamaterial, electromagnetic bandgap structures, and magnetic resonance imaging safety.



Abdul Basir (S'18–S'19) received the B.Sc. degree in telecommunication engineering from the University of Engineering and Technology, Peshawar, Pakistan, in 2015. He is currently working toward the M.S. degree in biomedical engineering with Hanyang University, Seoul, South Korea.

His research interests include implantable antennas and systems, biomedical circuits, wearable antennas, multiple-input multiple-output communication, metamaterial, dielectric resonator antennas, reconfigurable antennas, long-range wireless power transfer, and wireless charging of biomedical implants.



Hyungsuk Yoo (M'18) received the B.Sc. degree in electrical engineering from Kyungpook National University, Daegu, South Korea, in 2003, and the M.Sc. and Ph.D. degrees in electrical engineering from the University of Minnesota, Minneapolis, MN, USA, in 2006 and 2009, respectively.

In 2009, he joined the Center for Magnetic Resonance Research, University of Minnesota, as a Postdoctoral Associate. In 2010, he joined Cardiac Rhythm Disease Management, Medtronic, MN, USA, as a Senior MRI Scientist. From 2011 to 2018, he was an Associate Professor with the Department of Biomedical Engineering, School of Electrical Engineering, University of Ulsan, Ulsan, South Korea. Since 2018, he has been an Associate Professor with the Department of Biomedical Engineering, Hanyang University, Seoul, South Korea. He has been the CEO of E2MR, a startup company, since 2017. His current research interests include electromagnetic theory, numerical methods in electromagnetics, metamaterials, antennas, implantable devices, and magnetic resonance imaging in high-magnetic-field systems.